Nearly-free-electron effective model for conducting nanotubes

C. E. Cordeiro,[1] A. Delfino,[1] and T. Frederico[2]
[1]*Instituto de Física, Universidade Federal Fluminense, Avenida Litorânea s/n, 24210-340 Niterói, Rio de Janeiro, Brazil*
[2]*Departamento de Física, Instituto Tecnológico de Aeronáutica, 12228-900 São José dos Campos, Brazil*
(Received 19 February 2008; revised manuscript received 20 November 2008; published 26 January 2009)

We study a nonrelativistic quantum-field-theory model of a many-fermion system on a small cylindrical surface. An attractive contact effective two-body interaction is assumed to permit binding of fermions on the surface. We treat the many-fermion system within mean-field thermodynamics. A self-consistent Hartree-Fock calculation is performed and the total energy, pressure, and chemical potential are investigated in a thermodynamically consistent way. The model is applied to study the electronic properties of metallic single-walled nanotubes (SWNTs). We derive an analytical relation for the single-particle energy separation between two consecutive spikes provoked by Van Hove singularities in the density of states. We also found that the effective electron-electron interaction is necessary to reproduce the experimental fluctuation of the work function as a function of the diameter of SWNTs. The experimental distribution of the work functions with radius presents a nontrivial left-right asymmetry around the peak value that is reproduced by the model. Also, for SWNTs with radius smaller than 2 Å, the model gives a work function that increases linearly with $1/R$.

DOI: 10.1103/PhysRevB.79.035417 PACS number(s): 61.46.Fg

I. INTRODUCTION

Carbon nanotubes (CNTs) are new tools for practical applications of quantum properties in the nanoworld. The interest of using CNTs in nanodevices, particularly in optoelectronics, micromechanics, molecular biology, and thin films, is in part motivated by the intense research of such systems under multiple and different conditions.[1] For example, CNTs can be used as gas sensors. Geometric effects are important for the absorption of gases by nanotube bundles as the gas can be absorbed in the interstitial site between nanotubes, in the external groove site, and in the external bundle surface.[2] In particular, the energy released by the atoms captured by the bundle or their binding depends on the geometry, e.g., when an atom is constrained to move on the nanotube surface of radius of few angstroms, its cohesion is enhanced as has been shown in Ref. 3.

Cylindrical geometry of nanotubes gives unique properties to an interacting quantum many-body system constrained its surface. In the case of neutral atoms adsorbed on the surface or even electrons, the knowledge of their thermodynamic properties is of current interest. Such a study, in the case of free electrons in confined space, with different kind of geometries, has already been performed.[4] In this case, the electrons form a free many-fermion system on the nanotube surface which characterizes a metallic behavior of the system. This indeed is possible, as pointed out by Baughman *et al.*[5] that single-walled nanotubes (SWNTs), consisting of a single graphite sheet seamlessly wrapped into a cylindrical tube, may be either metallic or semiconducting, depending on the sheet direction about which the graphite sheet is rolled to form a nanotube cylinder. This fascinating subject is theoretically studied by tight-binding models and first-principles calculations (see, e.g., review in Ref. 6). However, if one aims to study coherent phenomena, e.g., superconductivity, the interaction between weakly localized electrons by either the Coulomb force or through the carbon lattice (both summarized in an effective potential) has to be considered in the description of the many-body system. Indeed metallic single-walled nanotubes are known for a long time and experimentally observed.[7] They can also show up as long ballistic conductors.[8]

Therefore, it seems necessary to face the difficult problem of calculating the contribution of an effective electron-electron interaction to the electronic properties of the weakly localized electrons, as they correspond to the charge carriers on the cylindrical surface. The interplay of geometry and interaction should provide unique properties to the many-electron system on the CNT surface. For example, one of these is the measured current saturation for single[9] and multiwalled CNTs.[10]

In this work we investigate the effect of the pairwise interaction in the single-particle properties of nonrelativistic many-fermion system with a constrained cylindrical geometry. This work can be separated in two parts. The first is the two-dimensional interacting N-fermion quantum-mechanical problem, formulated as nonrelativistic quantum-field-theory model on a cylindrical surface with a pairwise interaction. The properties of the ground state of the system of N fermions are solved in the Hartree-Fock (HF) approximation. The thermodynamical equations of state (EOSs) at zero temperature are derived analytically and the quantum-size effects conceptually discussed and illustrated. At least from our knowledge such a study has not been presented before. The second issue is whether such a model can be used to investigate the properties of weakly localized electrons on a nanotube surface.

As a simple step in the ambitious program to study CNT electronic properties, we will address the second issue with a nonrelativistic quantum field model of the many-fermion system with an effective local two-body interaction depending on strength λ. The tubes are assumed to be neutral, hence, the positive nucleus charge density is equal in magnitude to the electron charge density, and thus, they do not contribute to the electron energy remaining the effective two-electron interaction as the dominant effect for the electron binding. The attractive effective interaction mimics the im-

portant physics from the atom-electron and electron-electron interaction within the many-body system (including, e.g., electron-phonon interactions). Nevertheless, it should reflect the main character that the electrons are bound on the surface, i.e., a net attraction on the surface. The chosen two-carrier interaction, for simplicity, is a point-coupling potential, turning out to exhibit a linear surface density dependence in the single-particle energy. In that respect the Hartree-Fock approximation of the single-particle energy of the many-electron system with the point-coupling interaction can be compared to the first-order contribution of the surface density in a density-functional theory.[11] In particular the work function (WF) within density-functional theory (DFT) is the magnitude of the single-particle energy of the highest occupied level in respect to the vacuum (see Ref. 12).

The model is parametrized to account for the experimental work function of a graphene sheet (see Ref. 13). In principle, such a parametrization becomes ambiguous since a family of interaction strength parameters (λ) and Fermi energies (E_F) is possible to reproduce the graphene work function. However, recent experimental data of the work function for 93 nanotubes widely distributed in a range of radius between 5 and 15 Å revealed a small radial dependence.[14] This experimental finding allowed us to choose E_F that fits the small radial dependence of the experimental work function. The model predicts an oscillatory behavior of the WF as a function of the radius. The experimental distribution of the work functions with radius presents a nontrivial left-right asymmetry around the peak value that is well reproduced by the model. This is the main achievement of our work. We also extend the calculations to study the work function for radii smaller than 5 Å. Let us remark that this region, called class II SWNT, has been investigated before for armchair, quasimetal, and semiconducting SWNTs with first-principles calculations.[15] Our model predicts a WF linear with $1/R$ for radii smaller than 5 Å.

The driven physics of the model are the delocalized electrons, the pairwise interaction, the constrained geometry, and due to that the Van Hove singularities (VHSs). As pointed out in Ref. 16 according to theoretical studies,[17] semiconducting (or metallic) SWNTs of similar diameters have a similar number of VHS near the Fermi level, independent of chiral angle. In this particular, with our model we obtain for a fixed diameter D an analytical relation for the energy separation between two consecutive peaks in the density of states (coming from VHS) as a function of the Fermi energy, showing a $1/D^2$ scaling. We will present results for the work function as a function of radius and Fermi energy.

We also study the zero-temperature thermodynamics of the problem. The pressure is obtained from the mean-field energy-momentum tensor as well as from the grand-canonical potential to verify the thermodynamical consistency. The behavior of the pressure as a function of the nanotube radius will be shown as well.

The work is organized as follows. In Sec. II, we present the model and the Hartree-Fock solution of the ground-state properties of the many-fermion system. We also provide a discussion of the model and its limitations in the perspective of the application to the many-electron system on the nanotube surface. In Sec. III, we present our study of the electronic properties of nanotubes with the model. In Sec. IV, we give our conclusions.

II. MODEL

Our aim in the following is to discuss a nonrelativistic quantum-field-theory (NRQFT) version of the well-known Walecka model,[18] already intensively studied in the context of relativistic nuclear matter. The NRQFT model for the electrons on the nanotube surface will be solved in the Hartree-Fock approximation. It is worthwhile to note that the Euler-Lagrange equation of motion for the fermion field operator, for the chosen nonrelativistic model Lagrangian, is given by the time-dependent Schrödinger equation with a nonlinear term, which also corresponds to the Heisenberg equation of motion.

A. Field theory formalism

We start with the following Lagrangian:

$$\mathcal{L} = \frac{i}{2}\psi^*\dot{\psi} - \frac{i}{2}\dot{\psi}^*\psi - \frac{1}{2m}\nabla\psi^*\cdot\nabla\psi - V(\psi^*,\psi), \tag{1}$$

in which $\hbar = 1$ and $\dot{\psi}$ indicates time derivative. By taking ψ and ψ^* as independent fields, the Euler-Lagrange equation furnishes

$$\frac{\partial\mathcal{L}}{\partial\psi^*} - \frac{\partial}{\partial t}\frac{\partial\mathcal{L}}{\partial\dot{\psi}^*} - \nabla\frac{\partial\mathcal{L}}{\partial\nabla\psi^*} = 0, \tag{2}$$

which leads to

$$-\frac{1}{2m}\nabla^2\psi + \frac{\partial V}{\partial\psi^*} = i\dot{\psi}. \tag{3}$$

The conjugate momenta are

$$\pi = \frac{\partial\mathcal{L}}{\partial\dot{\psi}} = \frac{i}{2}\psi^*, \quad \pi^* = \frac{\partial\mathcal{L}}{\partial\dot{\psi}^*} = -\frac{i}{2}\psi. \tag{4}$$

From the above equations, the Hamiltonian density, $\mathcal{H} = \pi\dot{\psi} + \pi^*\dot{\psi}^* - \mathcal{L}$, reads

$$\mathcal{H} = \frac{1}{2m}\nabla\psi^*\cdot\nabla\psi + V(\psi^*,\psi), \tag{5}$$

which also can be obtained through the zero component of the energy-momentum tensor,

$$T^{\mu\nu} = \frac{\partial\mathcal{L}}{\partial\partial_\mu\psi}\partial^\nu\psi + \partial^\nu\psi^*\frac{\partial\mathcal{L}}{\partial\partial_\mu\psi^*} - g^{\mu\nu}\mathcal{L}. \tag{6}$$

For a uniform system in equilibrium at rest, this tensor acquires the form

$$T^{\mu\nu} = (P+\mathcal{E})u^\mu u^\nu - Pg^{\mu\nu}, \tag{7}$$

where P is the pressure, $\mathcal{E}$ is the energy density, and u^μ is the four velocity of the fluid. As one can see, T^{00} is the same as the Hamiltonian density and $T^{ii} = P$.

In this paper, we present calculations with a Hermitian point-coupling interaction, $V(\psi^*,\psi) = \frac{\lambda}{2}|\psi(\vec{r})|^4$, but the proce-

dure could be extended to a more general interaction as, for instance,

$$V(\psi^*,\psi)=\frac{1}{2}\int d\vec{r}'\,\psi^*(\vec{r})\psi^*(\vec{r}')v(\vec{r}'-\vec{r})\psi(\vec{r}')\psi(\vec{r}), \quad (8)$$

where $v(\vec{r})$ being a local two-body potential. The quantization of this model for fermions amounts to impose anticommutation rules for the field operator acting on the Fock space, i.e.,

$$\{\psi_{s'}(\vec{r}'),\psi_s^\dagger(\vec{r})\}=\delta_{s's}\delta(\vec{r}'-\vec{r}), \quad \{\psi_{s'}(\vec{r}'),\psi_s(\vec{r})\}=0, \quad (9)$$

where the subindex s indicates the spin state. The Hamiltonian operator reads

$$H=\sum_{\text{spin}}\int d\vec{r}\left[\frac{1}{2m}\nabla\psi_s^\dagger(\vec{r})\cdot\nabla\psi_s(\vec{r})+\frac{1}{2}\int d\vec{r}'\,\psi_{s_1'}^\dagger(\vec{r})\psi_{s_2'}^\dagger(\vec{r}')\times\langle s_1's_2'|v(\vec{r}'-\vec{r})|s_1s_2\rangle\psi_{s_2}(\vec{r}')\psi_{s_1}(\vec{r})\right] \quad (10)$$

for a general local two-body potential depending also on the spin state of the particles, with matrix elements $\langle s_1's_2'|v(\vec{r}'-\vec{r})|s_1s_2\rangle$. In the present model, we assume s-wave contact interaction in singlet spin states, with matrix element

$$\langle s_1's_2'|v(\vec{r}'-\vec{r})|s_1s_2\rangle=\frac{\lambda}{2}\langle s_1's_2'|00\rangle\delta(\vec{r}'-\vec{r})\langle 00|s_1s_2\rangle, \quad (11)$$

where $\langle s_1s_2|SM\rangle$ is the Clebsh-Gordan coefficient.

B. Mean-field approximation

The Hartree-Fock variational equations are used to evaluate the wave function of the ground state of the Fermi gas on the nanotube surface. The matrix element of the Hamiltonian in the Slater determinant state is denoted as $\langle H\rangle=\langle K\rangle+\langle V\rangle$, with K and V being, respectively, the kinetic and potential-energy operators. The matrix element of the kinetic-energy one-body operator is

$$\langle K\rangle=-\frac{1}{2m}\sum_\alpha\int d\vec{r}\,\alpha_s^*(\vec{r})\nabla^2\alpha_s(\vec{r}), \quad (12)$$

and the mean value, or matrix element, of the potential energy for the two-body contact interaction in the singlet state is

$$\langle V\rangle=\lambda\sum_{\alpha\beta}\int d\vec{r}|\alpha_s(\vec{r})|^2|\beta_{-s}(\vec{r})|^2. \quad (13)$$

The stationary point of the variation in the functional

$$F[\alpha]=\langle H\rangle-\sum_\alpha\epsilon_\alpha\int d\vec{r}|\alpha_s(\vec{r})|^2 \quad (14)$$

gives the HF eigenvalue equation for the single-particle states

$$-\frac{1}{2m}\nabla^2\alpha_s(\vec{r})+2\lambda\sum_\beta|\beta_{-s}(\vec{r})|^2\alpha_s(\vec{r})=\epsilon_\alpha\alpha_s(\vec{r}). \quad (15)$$

In Eqs. (12)–(15) above, $\alpha_s(\vec{r})$ and $\beta_s(\vec{r})$ are single-particle state wave functions. The single-particle energy corresponding to $\alpha_s(\vec{r})$ is ϵ_α. The subindex s indicates the spin state.

In the nanotube geometry the fermions are constrained to move on the cylindrical surface. The appropriate coordinates are the position along the nanotube symmetry axis (z) and the angle in the transverse plane (θ). The normalized plane-wave solution of the HF equation in a spin state σ with periodic boundary condition in θ is

$$\alpha_s(\vec{r})=\frac{\delta_{\sigma,s}}{\sqrt{(A)}}e^{ik_zz}e^{in\theta}, \quad (16)$$

with $A=2\pi RL$, where R and L are, respectively, the radius and length of the nanotube. The integer n runs from $-\infty$ to $+\infty$. The single-particle energies are given by

$$\epsilon_k=\frac{k_z^2}{2m}+\frac{n^2}{2mR^2}+\lambda\sigma, \quad (17)$$

where fermion surface density is $\sigma=N/A$, with the number of particles

$$N=\sum_s\int d\vec{r}\langle\psi_s^\dagger(\vec{r})\psi_s(\vec{r})\rangle=\sum_\beta\int d\vec{r}|\beta_s(\vec{r})|^2=2\sum_n\frac{L}{2\pi}\int dk_z\theta(k_F-k), \quad (18)$$

obtained for each given Fermi momentum k_F. The wave number is $k=\sqrt{k_z^2+(n/R)^2}$. We are assuming a simple Fermi surface which embodies isotropy when the nanotube radius goes toward infinite, and the planar geometry is recovered.

The number of particles is given by

$$N=\frac{2L}{\pi}\sum_{|n|\le n_{\max}}\sqrt{k_F^2-\frac{n^2}{R^2}}, \quad (19)$$

where $n_{\max}$ is the highest integer smaller than k_FR. The density of states for a single-particle energy is

$$\frac{\partial N}{\partial\epsilon_k}=\frac{2L}{\pi}\frac{\partial}{\partial\epsilon_k}\sum_{|n|\le n_{\max,k}}\sqrt{2m\epsilon_k-\frac{n^2}{R^2}-\lambda\sigma}=\frac{2L}{\pi}\sum_{|n|\le n_{\max,k}}\frac{m\epsilon_k}{\sqrt{2m\epsilon_k-\frac{n^2}{R^2}-\lambda\sigma}}, \quad (20)$$

where $n_{\max,k}$ is the largest integer smaller than $\sqrt{2m\epsilon_k-\lambda\sigma}R$.

The kinetic part of the Hamiltonian reads

$$\langle K\rangle=\frac{L}{\pi}\sum_n\int dk_z\left(\frac{k_z^2}{2m}+\frac{n^2}{2mR^2}\right)\theta(k_F-k). \quad (21)$$

By performing the integration, the kinetic energy becomes

$$\langle K\rangle = \frac{L}{\pi}\sum_{|n|\le n_{\max}} \frac{1}{3m}\left(k_F^2 + 2\frac{n^2}{R^2}\right)\sqrt{k_F^2 - \frac{n^2}{R^2}}. \quad (22)$$

Substituting the single-particle states in the expression for $\langle V\rangle$, one has

$$\langle V\rangle = \lambda\frac{2}{A}\left(\frac{L}{2\pi}\sum_n \int dk_z \theta(k_F - k)\right)^2 = \frac{\lambda}{2}\sigma N. \quad (23)$$

At this point we have had the total energy

$$E = \langle H\rangle = \langle K\rangle + \langle V\rangle. \quad (24)$$

The total energy per particle e and the density energy $\mathcal{E}$ are so defined,

$$e = \frac{E}{N}, \quad \mathcal{E} = \frac{E}{A}. \quad (25)$$

The extremum of the surface energy density appears for a certain value of $k_F = k_F^o$ that has a vanishing derivative, which is written is terms of the dependence on k_F as

$$\frac{\partial}{\partial k_F}\left(\frac{\langle K\rangle}{N} + \frac{\langle V\rangle}{N}\right)\bigg|_{k_F = k_F^o} = 0. \quad (26)$$

This condition can be rewritten as

$$\lambda = \lambda_o = \frac{2A}{N_o}\left(\frac{\langle K\rangle_o}{N_o} - \frac{k_F^{o2}}{2m}\right), \quad (27)$$

where $\langle K\rangle_o$ and N_o stand for $\langle K\rangle$ and N at the point $k_F = k_F^o$. If one imposes the validity of Eq. (27), λ becomes a function of R. In the specific examples of nanotubes that will be discussed in Sec. III and for the parameters used for realistic cases, the N-electron system does not saturate. However, the value of λ obtained from Eq. (27) is not far from our parametrization of SWNTs. Let us remark that the kinetic and interaction energies become competitive in this case.

C. Thermodynamical approach

We begin the analysis of the thermodynamical properties of the model by obtaining the pressure from the energy-momentum tensor,

$$T^{ii} = \frac{\partial \mathcal{L}}{\partial \partial_i \psi}\partial_i \psi + \partial_i \psi^\dagger \frac{\partial \mathcal{L}}{\partial \partial_i \psi^\dagger} + \mathcal{L}. \quad (28)$$

We evaluate the matrix element of the energy-momentum operator, T^{ii}, in the Heisenberg picture using the Lagrangian density $\mathcal{L}$ from Eq. (1). The time dependence of the field operator $\psi(\vec{r},t)$ is given by $e^{-i\epsilon_k t}$, obtained in the HF approximation, where ϵ_k is the single-particle energy. Then we get that

$$\langle T^{zz}\rangle = \langle \mathcal{L}\rangle - \frac{1}{m}\langle \partial_z \psi^\dagger \partial_z \psi\rangle \quad (29)$$

and

$$\langle T^{\theta\theta}\rangle = \langle \mathcal{L}\rangle - \frac{1}{mR^2}\langle \partial_\theta \psi^\dagger \partial_\theta \psi\rangle, \quad (30)$$

where the matrix element of the Lagrangian operator in the Slater determinant state is given by

$$\langle \mathcal{L}\rangle = \left\langle \frac{i}{2}\psi^\dagger \dot{\psi} - \frac{i}{2}\dot{\psi}^\dagger \psi\right\rangle - \langle \mathcal{H}\rangle = \frac{L}{\pi A}\sum_n \int dk_z \epsilon_k \theta(k_F - k) - \langle \mathcal{H}\rangle = -\frac{\lambda}{2}\sigma^2. \quad (31)$$

After some straightforward manipulations, the matrix element of the spatial components of the energy-momentum tensor operator can be given by the simplified expressions,

$$\langle T^{zz}\rangle = \frac{\lambda}{2}\sigma^2 + \frac{2}{3}\frac{L}{\pi m A}\sum_{|n|\le n_{\max}}\left(k_F^2 - \frac{n^2}{R^2}\right)^{3/2} \quad (32)$$

and

$$\langle T^{\theta\theta}\rangle = \frac{\lambda}{2}\sigma^2 + \frac{2L}{\pi m A R^2}\sum_{|n|\le n_{\max}} n^2\left(k_F^2 - \frac{n^2}{R^2}\right)^{1/2}. \quad (33)$$

If one wants to study in a more general way the consistency of the model, the above quantities will help in checking the results derived with different thermodynamical ensembles. The components of the energy-momentum tensor are associated to the system pressure P as we will see in the following. Let us first define and calculate the chemical potential by using Eqs. (19) and (24),

$$\mu = \frac{\partial E}{\partial N} = \frac{\partial E/\partial k_F}{\partial N/\partial k_F} = E_F + \lambda\sigma. \quad (34)$$

It corresponds to the energy needed to remove or to add a particle to the many-body system. The above quantity can be related to the pressure if one proceeds rewriting the chemical potential as follows:

$$\frac{\partial E}{\partial N} = \frac{\partial \mathcal{E}}{\partial \sigma} = \frac{\partial (E/A)}{\partial (N/A)} = -\frac{A}{N}\left(-\frac{E}{A} + \frac{\partial E}{\partial A}\right) = -\frac{1}{\sigma}\left(-\mathcal{E} + \frac{\partial E}{\partial A}\right). \quad (35)$$

The usual definition of $P = -\partial E/\partial A$ for a fixed number of particles leads to

$$-P = \mathcal{E} - \mu\sigma. \quad (36)$$

This general thermodynamical relation when applied for our model gives

$$P = (E_F + \lambda\sigma)\sigma - \frac{\langle K\rangle}{A} - \frac{\langle V\rangle}{A} = E_F\sigma - \frac{\langle K\rangle}{A} + \frac{1}{2}\lambda\sigma^2. \quad (37)$$

After careful manipulation of terms and by introducing Eqs. (19), (22), and (23) into Eq. (37) one gets exactly T^{zz}, i.e., the energy-momentum tensor component presented in Eq. (32). This checks the thermodynamical consistency of our field theoretical derivation of the pressure. As a further remark, the condition of zero pressure $P = T^{zz} = 0$, i.e., hydrostatic

equilibrium, leads to the same extreme $\lambda=\lambda_o$, obtained in Eq. (27).

We call attention here that $T^{\theta\theta}$ is related to the change in the total energy with the radius. As the radius increases a planar structure is approached and $T^{\theta\theta}$ tends to T^{zz}. This conjecture can be seen analytically if we take the limit to large values of R in the last terms of Eqs. (32) and (33). The explicit sum of Eq. (32) gives $n_{\max}k_F$ while that for Eq. (33) becomes $n_{\max}(n_{\max}+1)(2n_{\max}+1)/6$. Considering $n_{\max}=k_FR$, the asymptotic results of Eqs. (32) and (33) are $T^{zz}=T^{\theta\theta}=\lambda\sigma^2/2+(2LR/3\pi mA)k_F^4$.

The inclusion of temperature in the model is also straightforward since basically the θ functions that we have employed in our derivation are, in fact, the zero-temperature limit of the finite-temperature Fermi distribution. Once the temperature is included, E_T and N will become temperature dependent and a grand-canonical thermodynamical potential may be defined as $-PA=E_T-TS-\mu N$, where S is the entropy.

D. Work function

In the following, we introduce the work-function definition within our model. As will be discussed in Sec. II D, in our model the two-body effective interaction, $\lambda\sigma$, is supposed to include all kind of correlations contributing to the energy functional. In this approximation, $\lambda\sigma$ is the well depth while E_F denotes kinetic energy of the electron in the Fermi level. For metals, it is a correct association. From the Wigner-Bardeen definition[19] the work function is given by the energy difference between a lattice with equal number of ions and electrons, and the same lattice with a removed electron. It is assumed, therefore, that the lowest electronic state is completely filled so that the electron is removed from the highest energy state of the neutral metal. However, in the case of insulator or semiconducting materials, one has to take into account the gap energy between valence and conduction bands. The Fermi level is, in general, not occupied by electrons and thus it acquires a more abstract meaning.

Although the proposed nearly-free-electron model does not include such effects in its present form, they may be extracted from other models. For instance, tight-binding empirical prediction for the band gap reads $E_g=|t|a_{c-c}/d$, where $d=2R$ is related to the chiral numbers $d=a\sqrt{n^2+m^2+nm}$. By choosing that, the Fermi-level should be redefined by including the midgap energy as a function of the nanotube radius R. For qualitative aims of the present work and considering that for large radii this contribution is actually too small; in what follows the work-function definition will not include the band-gap energy.

Therefore, in our model, the WF is defined as

$$\mathrm{WF}=E_F+\lambda\sigma, \tag{38}$$

with E_F being the electron kinetic energy at the top of the Fermi sea, and not at midgap, which is the usual for semiconducting nanotubes.[20] This definition turns out to be the same of the chemical potential [Eq. (34)], which is negative for bound systems. The work function defined above, in agreement with Eqs. (36) and (37), can as well be written as

$$\mathrm{WF}=\mu=\frac{\mathcal{E}}{N}+P\frac{A}{N}, \tag{39}$$

with its modulus interpreted as the energy necessary to remove a particle from the system that needs to overcome the bulk energy per particle and a pressure term, interpreted as a surface-potential step. Hereafter, when we apply the model we will present the magnitude of WF. As a remark, Eq. (39) is identical to our previous Eq. (36), which is the content of the Hugenholtz–Van Hove theorem.[21]

The identification of the surface-potential step as the pressure term is based on a recent work.[22] It pointed out that the difference between the chemical potential, interpreted as the total energy necessary to add or remove a particle from the many-electron system, and the energy per particle is exactly the electrostatic potential step at the surface. In that work, the potential step from the surface dipole was clearly related to the pressure, making our interpretation of the work function consistent.

Last but not least, some words about the Fermi energy level in our model are in order. The value set for this level is usually arbitrary and is chosen by convenience, although it is not unrelated to the band-structure energies. In Sec. III, when we apply our model, E_F will become a parameter in order that our work function fits the experimental data. In this case, Eq. (38) can be interpreted as $\mathrm{WF}=(E_F-V_{\mathrm{ref}})+(\lambda\sigma+V_{\mathrm{ref}})$, where the reference energy, V_{ref}, varies for different nanotubes. For practical purposes, however, we do not need to know the explicit value of V_{ref} since E_F already parametrizes the model. The limitations of our model will be thoroughly discussed in Sec. II E. If we define a dimensionless parameter $x=k_FR$, the work function can be cast in the following form:

$$\mathrm{WF}=E_F\left(1+\frac{2m\lambda}{\pi^2x}\sum_{|n|\le n_{\max}}\sqrt{1-\frac{n^2}{x^2}}\right). \tag{40}$$

This form is convenient to analyze the case $x=k_FR<1$ and the asymptotic limit $x=k_FR\gg 1$. In the last case, the x dependence in Eq. (40) goes to $\pi/2$, giving for WF and $\sigma=N/(2\pi RL)$ the following asymptotic behavior:

$$\lim_{x\to\infty}\mathrm{WF}=E_F\left(1+\frac{mc^2\lambda}{\pi(\hbar c)^2}\right), \tag{41}$$

and electron surface density tends to

$$\lim_{x\to\infty}\sigma\ (\text{Å}^{-2})=\frac{k_F^2}{2\pi}=\frac{mc^2}{\pi(\hbar c)^2}E_F=0.042E_F\ (\mathrm{eV}), \tag{42}$$

where we have shown explicitly the factors $\hbar$ and the light speed c. Note that $\hbar c=1973$ eV Å and for electrons $mc^2=0.511\times10^6$ eV. So, $k_F=\sqrt{2mc^2E_F/(\hbar c)^2}=0.51\sqrt{E_F}$ (eV) in units of Å^{-1}. Therefore, $x=0.51\sqrt{E_F}\ (\mathrm{eV})R$ (Å). The asymptotic expression for the work function [Eq. (41)] allows an asymptotic strength parameter,

$$\lambda(E_F) = \frac{\pi(\hbar c)^2}{mc^2}\left(\frac{\mathrm{WF}}{E_F} - 1\right), \tag{43}$$

which may become useful even for $x=k_FR$ for values not necessarily too large, provided the work function has a small radial dependence.[14] Indeed, we will see in our applications that to have a good approximation between the exact expression for WF and σ to the asymptotic expressions given by Eqs. (41) and (42), $x \approx 5$, should be enough. From Eq. (42) we also see in a clear form how the Fermi level modulates the carrier concentration.

E. Some considerations about the model and its limitations

At this point is important to put the model and our approximations in the perspective of the complexity of the many-electron system on the nanotube surface. In order to apply model Lagrangian (1) in that case, we use an effective contact two-electron interaction depending on a strength λ. We stress that effective two-body potential (8) should be distinguished from the bare repulsive Coulomb potential, as it parametrizes all kind of correlations that contributes to the energy functional. Seen in this way, the correlations are included, albeit in a simplified form, in what it is formally presented as the HF ground-state energies and densities in a mean-field calculation (see Ref. 23). However, it is hard to distinguish the contribution of a particular correlation to the energy functional. The long-range many-body correlations with contributions to the energy functional that are in the form of powers and gradients of σ could be included in our model by a density dependent λ, and by introducing in Lagrangian density (1) one-body terms with higher derivatives of the fermion field. Indeed in the nuclear physics context the Skyrme functional, in the spirit of an effective model, includes several of these terms with adjustable parameters (see discussion in Ref. 23). In that respect the Hartree-Fock approximation of the single-particle energy of the many-electron system with the point-coupling interaction can be compared to the first-order contribution of the surface density in a density-functional theory.[11] We have to point that when fitting the model parameters to the work function of graphene, we cannot separate *a priori* the HF part from correlation contributions. Thus, our model parameters as obtained from the fitting procedure to the graphene work function brings to the electron properties on the nanotube surface correlations beyond the HF calculation.

In our model the strength of contact interaction (11) should be in general a functional of the density itself. Such dependency parametrizes the contribution of correlations to the energy functional, which also means a nonconstant strength for SWCNT with different radius. We will assume that the dependency is small for large nanotube radius as we will fit the work function of the graphene sheet. For small nanotube radius the effective interaction increases, an effect that is missing in our model. As we will see by the comparison with the experimental data of the work function for $D > 10$ Å, this effect can be ignored, while for small radius nanotubes the model deviates from *ab initio* calculations as shown in Sec. III.

The SWCNT is assumed to be neutral, hence, the positive nucleus charge density is equal in magnitude to the electron charge density, and thus, they do not contribute to the energy functional remaining only the effective two-electron potential as the dominant interaction in the electron binding. This assumption also suggests that the effect of the lattice structure in the dispersion relation of the electron is small, although it is know that for metallic SWCNT the energy depends linearly on the momentum especially near the "K" points. However, on these particular points, it is important to remind the reader that the linearity in the dispersion relation corresponds to the tangent to the free dispersion relation.

The involucre of the dispersion relation is approximately given by the free kinetic energy, as indicated by the overall neutrality of the nanotube surface. Therefore, the Fermi momentum of last filled level can be extracted by the kinetic energy of the last filled level. Indeed, in the comparison with the experimental data for the work function as we will show, it is required the relation between the Fermi kinetic energy and Fermi momentum. It is also reasonable to expect that the error in the evaluation of the Fermi momentum from the value of the free kinetic energy should be small. Moreover, the maximum electron kinetic energy that is limited by the Fermi wavelength gives a finite width for the filled bands for momentum along the nanotube symmetry axis and for all one-dimensional (1D) subbands originated by wrapping the graphene sheet. An improvement of the model should include the lattice structure in the evaluation of the electron dispersion relation, which will be left for a future work.

III. RESULTS AND DISCUSSION

The model we have presented is a very simple one. Once the radius R and the length L of the cylinder are given, the number of fermions N is obtained from Eq. (19) as a function of the Fermi energy $E_F=k_F^2/2m$. Let us remark that N as well as the surface density $\sigma=N/2\pi RL$ do not depend on fermion interaction details. Both are basically controlled by the cylinder radius R and the Fermi energy surface E_F. Nevertheless as we will see, a substantial physics content of very small quantum systems is built in their kinematics and geometry themselves. Therefore, R plays a crucial role in the quantum behavior of the fermions on the surface once the maximum value of the quantum number n is limited by $x=k_FR$ [see Eq. (19)]. This property is reflected in the oscillatory behavior of the kinetic energy as a function of R or E_F. Also the jump from n to $n+1$ causes the Van Hove singularities in the density of states near the Fermi surface [see Eq. (20)]. The density of states [Eq. (20)], the total energy per particle e [Eq. (25)], the pressure [Eq. (37)], and the work function [Eq. (38)] depend on R, E_F, and λ. The strength of the interaction, λ, is a free parameter to be eliminated in favor of some specific measured observable for a known Fermi energy. To describe the properties of carbon SWNTs we fit λ to reproduce a work function around 4.8 eV with small fluctuations for a large range of radius values.[14] This condition constraints only the pair of values (λ, E_F), i.e., λ appears as a function of E_F for a given work function.

Here we will discuss our parametrization procedure in more detail. Let us first clarify that different (λ, E_F) sets may

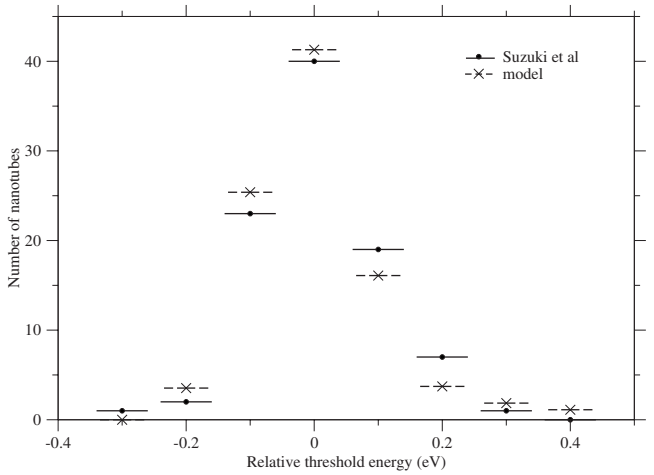

FIG. 1. Number of nanotubes as a function of the relative threshold energy for thousand equally spaced radius from $R=5$ Å to $R=15$ Å and normalized to 93 events. The model parameters are given in the text.

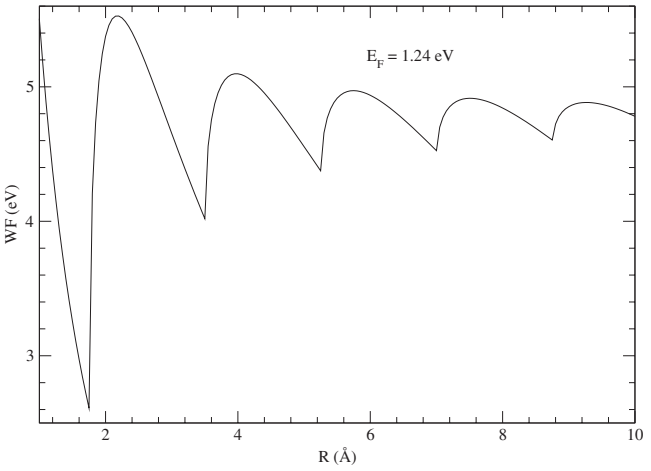

FIG. 2. Work function with varying radius for a fixed $E_F=1.24$ eV.

lead to the same expected work function of about ≈4.8 eV. This can be easily seen from Eq. (40) or its asymptotic form [Eq. (27)]. By knowing this, we have chosen an optimal (λ, E_F) set which takes into account not only the asymptotic value of the experimental work-function data but also the oscillations around the average.

By analyzing 93 SWNTs widely distributed in a range of radius between 5–15 Å, Suzuki *et al.*[14] measured the radial dependence of the work function. They classify the nanotubes according to the WF values around the average in the intervals [−0.05 eV, +0.05 eV], [+0.05 eV, +0.15 eV], [−0.05 eV, −0.15 eV], [−0.15 eV, −0.25 eV], [+0.15 eV, +0.25 eV], [−0.25 eV, −0.35 eV], and [+0.25 eV, +0.35 eV]. The data were presented as a histogram for the number of nanotubes within each interval of value of the work function. To compare the results of our model with the experimental data, we choose an interval of values of R and attribute equal probability for nanotubes having a radius in the whole range of radii between 5 and 15 Å. We set the grid points on R to allow the calculation of thousand WFs in that interval of values. With this, we obtain the average value of the work function for $5<R<15$ Å. To calculate the fluctuation of the WF around the mean value, we count the number of nanotubes having a variation in the WF with respect to the mean value inside the intervals used to classify the experimental data.

In the numerical evaluations we use $L=1\,000$ Å. An optimal set parameter was obtained for $E_F=1.24$ eV and $\lambda=-116.61$ eV Å^2. Our results, for thousand equally spaced radius from $R=5$ Å to $R=15$ Å and normalized to 93 events are presented by the histogram of Fig. 1. The model reproduces nicely the experimental data. This shows that the model is able to be fine tuned to the details of the histogram.

How we have obtained this fitting deserves a comment as follows. The experimental work-function data show small radial fluctuations. From theoretical quantum-size effect prediction of the model—see, for instance, Eqs. (19), (20), and (40)—the amplitude of the oscillation of the WF around the average decreases as the radius increases, i.e., $n_{\max}$, becomes higher. Therefore, the more the radius increases, the less the work function fluctuates from its average value. In this perspective, the average work-function value goes fast to the asymptotic result. Indeed, our λ has been obtained from the asymptotic expression [Eq. (43)], with WF=4.8 eV and $E_F=1.24$ eV. Note here that the change of $E_F=1.24$ eV to another value does not modify the asymptotic or the average work-function value taken as WF=4.8 eV but only the fluctuations around this value.

That is why we call our choice or $E_F=1.24$ eV as optimal since it reproduces nicely the oscillation found for the experimental work-function data. However, we should stress that the experimental distribution of the work functions with radius shows a nontrivial left-right asymmetry around the peak value that is well described by the model once the peak value of the histogram and graphene work function are fitted. This is the main achievement of our work. In Fig. 2 we can see the work-function dependence on the radius as predicted by the model with $E_F=1.24$ eV.

Still discussing Figs. 1 and 2 we point out the average value of WF=4.798 eV to be compared with WF=4.8 eV, the graphene work function asymptotic one. To get the average value, the Fermi shells controlled by $n_{\max}$ runs from 3 to 8. The model gives for the quasifree electrons a surface density of ≈0.05 Å^2.

In Fig. 3 we show the dependence of the work function with the Fermi energy for a fixed radius, $R=5$ Å. This figure also shows that the work function oscillates around the average and the asymptotic value. Note that $n_{\max}$ is the quantum number of the last shell with electrons [see, for instance, Eq. (40)], and we recall that it is given by the largest integer smaller than $k_F R=x=0.51\sqrt{E_F\ (\mathrm{eV})}R\ (\text{Å})$. The jump from one shell to the next one originates the oscillating pattern shown in Figs. 1 and 2.

Now, we will show the behavior of other physical quantities derived from the model with the previous parametrization. In Fig. 4 we show the density of states at the Fermi surface given by Eq. (20) as a function of the nanotube radius. If we analyze more carefully the oscillations we find a defined period and a common $1/R$ decaying rate. Such be-

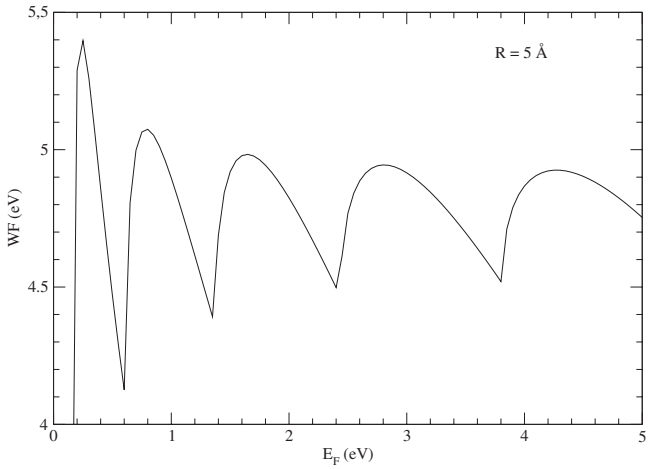

FIG. 3. Work function as a function of Fermi energy for $R=5$ Å with λ given by Eq. (43).

havior has already been theoretically studied in Ref. 24 for metallic carbon nanotubes in which the Van Hove singularities were interpreted in analogy to the de Haas–van Alphen effect. In that study, using Green's-function approach within a tight-binding model, they showed the appearance of radial oscillations in the electronic properties of the nanotube.

The peaks of the density of states in Fig. 4 are associated to the Van Hove singularities. From our model, it is also possible to derive an analytical expression for the radius at which the density of state peaks [see Eq. (20)],

$$R_k = \frac{(\hbar c)k}{[2mc^2(E_F - \lambda\sigma)]^{1/2}} = \frac{(\hbar c)k}{[2mc^2(2E_F - \mathrm{WF})]^{1/2}}, \quad (44)$$

where $k=1,2,3,\ldots$ stands for the available shells. This expression relates the Van Hove singularity at a given nanotube radius with the Fermi energy and the work function.

The qualitative features of the density of states seen in our Fig. 4 and those in Ref. 24 are quite similar as they are dominated by the jump from one filled shell to the next one. As we see, the density of states at the Fermi energy is very

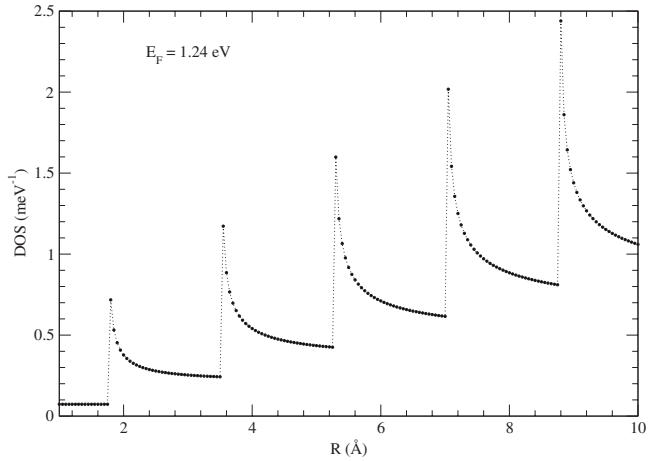

FIG. 4. Density of states at the Fermi surface as a function of the radius.

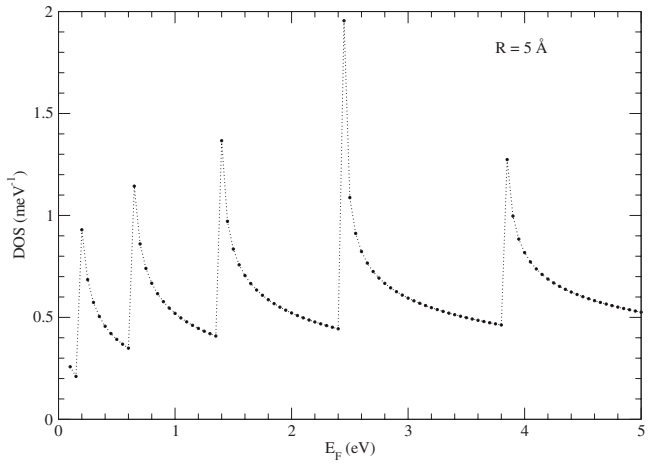

FIG. 5. Density of states as a function of the Fermi energy for $R=5$ Å.

sensitive to the radius of the cylinder due to the dependence with $n_{\max}$ (the largest integer smaller than $k_F R$). Therefore, when R is too small, only few quantum states in Fermi sea are filled. In the case of Fig. 4, $n_{\max}$ changes from 1 to 5 when R goes from 2 to 10 Å. In the extreme case, decreasing further the radius to $R<2$ Å, $n_{\max}=0$, the system becomes a one-dimensional nanowire. In the opposite limit, when R becomes very large, not shown in Fig. 4, the cylindrical surface becomes a planar structure of the graphene sheet.[25]

In Fig. 5 it is shown the density of states as a function of the Fermi energy for $R=5$ Å. Again, oscillations occur. In our model, the energy separation between two consecutive peaks in the density of states as a function of the Fermi energy, for a fixed radius and λ, from Eq. (20), reads

$$\Delta E^{(j)} = E^{(j)} - E^{(j-1)} = \frac{(\hbar c)^2 j}{mc^2 R^2} - \frac{1}{2mR^2} + \frac{\lambda}{\pi R^2}\left(\sum_{|n|\le j-1}\sqrt{j^2-n^2} - \sum_{|n|\le j-2}\sqrt{(j-1)^2-n^2}\right), \quad (45)$$

where $E^{(j)}=(\hbar k_F^{(j)})^2/2m+\lambda\sigma^{(j)}$. For large values of integer j the above equation can be simplified,

$$\Delta E^{(j)} \approx \frac{(\hbar c)^2 j}{mc^2 R^2} + \frac{\lambda(2j)^{1/2}}{\pi^2 R^2}, \quad (46)$$

showing a scaling of $\Delta E^{(j)}$ with $1/R^2$.

In the following we present the thermodynamical properties of the electronic system on the nanotube surface. In Fig. 6 we show the total energy per particle (e) given by Eq. (25). The oscillation of the total energy and other quantities as a function of R and/or E_F is expected to happen as a consequence of the oscillation in the density of states. Indeed, we see an oscillatory behavior of the energy per particle by varying the cylinder radius. The same also happens if we use the parameters of Fig. 3 to calculate the energy per particle as a function of the Fermi energy.

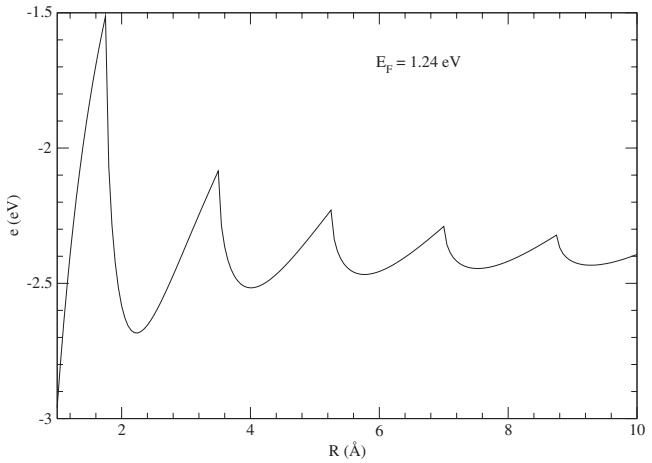

FIG. 6. Total energy per particle as a function of the radius with the same parameters used in Fig. 1.

A new outcome of our model is shown in Fig. 7, where we present results for the energy-momentum tensor components T^{zz} and $T^{\theta\theta}$. As we have analytically shown in the previous section, T^{zz} is equal to the thermodynamic pressure given by Eq. (37). This plot exhibits how $T^{\theta\theta}$ approaches T^{zz} as the radius increases according to what we have analytically shown before. Here, we notice how fast both $T^{\theta\theta}$ and T^{zz} approach to each other already for radii of few angstroms. In the limit of large radius, i.e., toward a flat graphene piece, the pressure could be actually given by $p=(T^{\theta\theta}+T^{zz})/2$, which is broken, at small radius, by the cylindrical symmetry.

Let us stress that despite our good fit of the work function seen in Fig. 1, the model is solved in a mean-field approximation and does not intend to be realistic in predicting properties for nanotubes for which a very rich band structure appears. Nevertheless, we expect that under the limitation of a nearly-free-electron model the right qualitative physics of the system is addressed. For a large set of parameters (λ, E_F) and $R>5$ Å we have a small radial dependence of the work function, as verified experimentally.[14] This robust property is deeply built into our effective model.

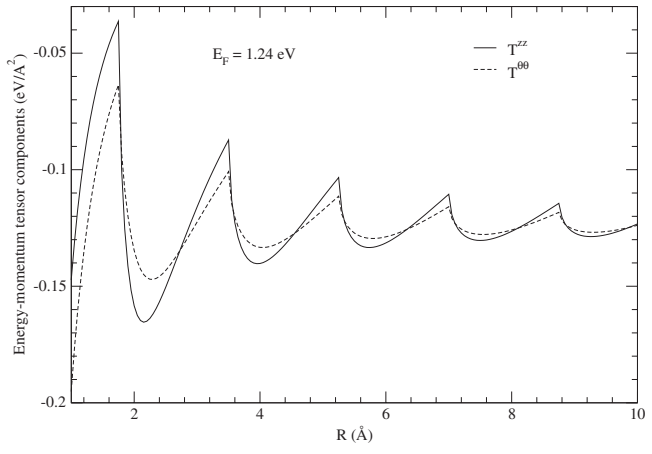

FIG. 7. Energy-momentum tensor components T^{zz} (full line) and $T^{\theta\theta}$ (dashed line) as a function of R for the same parameters of Fig. 1.

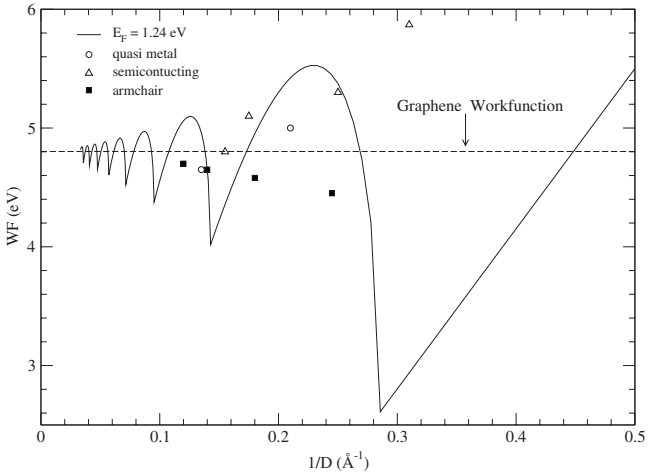

FIG. 8. Work-function dependence with $1/D$ for our model compared to the calculations from Ref. 15.

Before we close this section it is necessary to remark that a first-principles calculation of SWNT work function[15] was performed for class I ($R>5$ Å) and class II ($R<5$ Å) nanotubes. In Fig. 8 we compare our results for the WF as a function of $1/D$ with calculations from Ref. 15 for armchair, quasimetal, and semiconducting SWNT. For class I, they found that the work function appears distributed within a narrow band of ≈ 0.1 eV with no significant chirality or radius dependence, while the experimental data of Suzuki *et al.* shows a larger band (see Fig. 1). In class II, those results for the work function show a substantial change depending on armchair or zigzag structure. Our model, without further refinements, which is left for a future work, does not distinguish the band details rather than those contained in the tube radius and Fermi energy. For the class I nanotubes the chirality seems not to be crucial for obtaining the work function since it appears in a narrow band around the graphene work function and also supported by the results of our model, as shown in Fig. 1. However, this is not the case for class II nanotubes, for which the work function results show a large amplitude oscillation also corroborated qualitatively by our model.

In Fig. 8 (see also Fig. 2) we observe a noticeable oscillation of the work function for $D<10$ Å. This is the region in which $n_{\max}<2$. In particular, in angstrom units, when $8<D<10$, $4<D<8$, and $D<4$, $n_{\max}=2,1,0$, respectively. The case $n_{\max}=0$ is particularly interesting once the work function [see Eq. (40)] becomes

$$\mathrm{WF} = E_F\left(1+\frac{2mc^2\lambda}{(\hbar c)^2\pi^2 x}\right), \tag{47}$$

which increases linearly with $1/x=1/(k_F R)$ for fixed E_F. Substituting in Eq. (47) the value of λ by the asymptotic $\lambda(E_F)$, given by Eq. (43), we can connect the results of $\mathrm{WF}(x<1)$ to those of $\mathrm{WF}(x\gg 1)$,

$$\mathrm{WF}(x<1) = E_F\left[1+\frac{4}{k_F\pi}\left(\frac{\mathrm{WF}(x\gg 1)}{E_F}-1\right)\frac{1}{D}\right], \tag{48}$$

which raises with $1/D$, clearly seen in Fig. 8 for D smaller than about 4 Å.

As we can see from Fig. 8, our model deviates strongly from the results in Ref. 15 for the semiconductor case where $D<4$ Å. Our model is parametrized to reproduce the average WF=4.8 eV for $D>10$ Å with $E_F=1.24$ eV. It is expected that our nearly-free-electron effective model fails to reproduce the first-principles calculations of the work function for semiconducting nanotubes. Our model has a fixed k_F; it misses the rich band structure and chirality-dependent properties, which seems to be crucial for the work function at small radius. Nevertheless, for class II nanotubes, with larger radius, our model was able to account for the left-right asymmetry seen in the histogram that presents the number of nanotubes with deviations of the WF from the average within given intervals as shown in Fig. 1. This fine tune result of the model is a direct consequence of Eq. (38) for the WF obtained in the Hartree-Fock approximation to the single-particle energy of the many-electron system with the point-coupling interaction. Therefore, we believe that for large nanotube radius the particular expression of the WF derived in this work goes beyond the limitations of the model. This expression could come from a first-order contribution of the surface density to the single-particle energy within DFT. Moreover, within DFT, the WF is the single-particle energy of the highest occupied level with respect to the vacuum.[12]

IV. CONCLUSIONS

We have studied the properties of an interacting N-fermion system on a cylindrical surface focusing in the quantum-mechanical size effects of the ground-state observables. Our first step was to construct a model based on nonrelativistic quantum field theory from which one can provide a consistent thermodynamical approach. We have done this by starting from a Lagrangian density which gives the energy density and ultimates in a nonrelativistic Hamiltonian operator. To quantize the model we have chosen an effective two-fermion point-coupling interaction, which in coordinate space is given in terms of a δ function in the relative distance between two fermions. However, the model can be implemented with a more general local interaction [see Eq. (8)]. To obtain the properties of the ground state, we use the well-known Hartree-Fock approximation, which made possible an analytic treatment of the problem. Here, it is interesting to remark that the single-particle energy in the Hartree-Fock approach for the point-coupling two-carrier interaction turned out to exhibit a linear surface density dependence compatible with a first-order contribution of a density-functional theory.[11] In this way, higher order terms that could appear in DFT could be simulated by including many-body point-coupling interactions treated in mean-field approximation.[26]

In addition, the thermodynamical properties were derived and the density of states, total energy, chemical potential, and the pressure were defined properly. Within this model, quantum-size effects can be understood as a consequence of filling states in the Fermi sea in which a clear dependence on the Fermi momentum and the nanotube radius naturally arises [see, e.g., Eq. (19)]. The model provides an interesting example to investigate the interplay between geometry and the quantum mechanics of interacting many-fermions systems. From our knowledge such a kind of example was not discussed in so many details as we have done here.

As an application, we used the model to study some electronic properties of nanotubes with metallic behavior. When the electrons are well localized in the carbon sites, one has, for instance, the validity of the widely used tight-binding approximation to model the electronic properties of the nanotube.[6] It is well known that this approximation is strongly based on the localization of the valence electrons at their atomic cores. The present model is in some sense complementary to that approximation since it describes a system of nearly-free electrons in long conducting nanotubes, where one expects that the tight-binding approximation may not work well.

We have calculated the density of states for fixed Fermi momentum as a function of the radius as well as for fixed radius as a function of the Fermi energy. In the first case, we found the values of the radius for which a Van Hove singularity occurs in terms of E_F and WF [see Eq. (44)]. In the second case, when the radius is fixed we found an analytical relation for the separation between the Fermi energies of two consecutive peaks due to Van Hove singularities in the density of states. From this relation we can see in a very clear form the kinematical and the dynamical contributions, both exhibiting a geometric scaling with $1/R^2$ [see Eq. (46)].

Our model has only one free parameter λ besides the Fermi energy. In our applications we have eliminated λ in favor of the experimental work function of the graphene sheet. We have found different (λ, E_F) for same the experimental work function. Indeed, in our model, the Fermi level modulates the electric carrier concentration as well as the values of λ, compatible to the experimental WF. The smaller is the Fermi energy the smaller is the charge-carrier concentration σ, which is λ independent. Here we remark that even for quite different pair of values (λ, E_F) fitting the graphene sheet WF, the variation in WF as a function of the nanotube radius is small for $R>5$ Å.

We studied the work function (WF) as a function of the radius with our model parametrized to reproduce the experimental WF average data around 4.8 eV from 0.5 nm to 1.5 nm.[14] The experimental data shows a WF with a small sensitivity to either the radius or chirality in this region. Indeed, as discussed in Sec. III, we have found a family of different values of λ and E_F fulfilling the constraint of small radius dependence. Following Ref. 14 we have also performed a more detailed study of the fluctuations of the WF around the mean value. Our model is able to account for the nontrivial left-right asymmetry of the histogram, which shows the number of nanotubes with deviations of the WF from the average within given intervals (see Fig. 1). This detailed fit of the model is a direct consequence of the simple expression of the WF as the Fermi energy plus the potential energy (proportional to the surface density) [Eq. (38)]. This relation was obtained in the Hartree-Fock approximation to the single-particle energy of the many-electron system with the point-coupling two-body interaction. Therefore, for large nanotube radius the simple form of the WF derived here goes beyond the limitations of the model. It could correspond to a first-order contribution of the surface density to the single-particle

energy within DFT. However, the nearly-free-electron effective model fails to reproduce the first-principles calculations of the work function for semiconducting nanotubes for radius below 5 Å. Our model has a fixed Fermi momentum and misses the rich band and chirality structures, which seems to be crucial for the work function at small radius. In this region, the Fermi level of semiconducting SWNT is easily shifted by adsorbates or defects,[27] and the semiconducting SWNT work function may be strongly dependent on the Fermi-level position in the band gap.

Temperature effects were not studied in our model. Qualitatively, however, we can presume that its appearance will favor the electron mobility, improving the nearly-free-electron approximation on which our model is physically based.

ACKNOWLEDGMENTS

The authors thank the useful discussions with L. K. Teles. The authors also would like to express their thanks to Conselho Nacional de Desenvolvimento Científico e Tecnológico (CNPq) and to Fundação de Amparo à Pesquisa do Estado de São Paulo (FAPESP) for partial financial support.

[1] R. Saito, G. Dresselhaus, and M. S. Dresselhaus, *Physical Properties of Carbon Nanotubes* (Imperial College, London, 1998).
[2] M. M. Calbi, M. W. Cole, S. M. Gattica, M. J. Bojan, and G. Stan, Rev. Mod. Phys. **73**, 857 (2001).
[3] M. K. Kostov, M. W. Cole, G. D. Mahan, C. Carraro, and M. L. Glasser, Phys. Rev. B **67**, 075403 (2003).
[4] W. S. Dai and Mi Xie, Phys. Rev. E **70**, 016103 (2004).
[5] R. H. Baughman, A. A. Zakhidov, and W. A. de Herr, Science **297**, 787 (2002).
[6] J.-C. Charlier, X. Blase, and S. Roche, Rev. Mod. Phys. **79**, 677 (2007).
[7] S. J. Tans, M. H. Devoret, H. Dai, A. Thess, R. E. Smalley, L. J. Geerligs, and C. Dekker, Nature (London) **386**, 474 (1997).
[8] C. T. White and T. N. Todorov, Nature (London) **393**, 240 (1998).
[9] Z. Yao, C. L. Kane, and C. Dekker, Phys. Rev. Lett. **84**, 2941 (2000).
[10] P. G. Collins, M. Hersam, M. Arnold, R. Martel, and Ph. Avouris, Phys. Rev. Lett. **86**, 3128 (2001).
[11] W. Kohn and L. J. Sham, Phys. Rev. **140**, A1133 (1965).
[12] C. O. Almbladh and U. von Barth, Phys. Rev. B **31**, 3231 (1985).
[13] S. Suzuki, S. Bower, Y. Watanabe, and O. Zhou, Appl. Phys. Lett. **76**, 4007 (2000).
[14] S. Suzuki, Y. Watanabe, Y. Homma, S. Fukuba, and A. Locatelli, Appl. Phys. Lett. **85**, 127 (2004).
[15] Bin Shan and Kyeongjae Cho, Phys. Rev. Lett. **94**, 236602 (2005).
[16] P. Kim, T. W. Odom, Jin-Lin Huang, and C. M. Lieber, Phys. Rev. Lett. **82**, 1225 (1999).
[17] C. T. White *et al.*, Nature (London) **394**, 29 (1998); J.-C. Charlier and P. Lambin, Phys. Rev. B **57**, R15037 (1998).
[18] B. D. Serot and J. D. Walecka, Adv. Nucl. Phys. **16**, 1 (1995).
[19] E. Wigner and J. Bardeen, Phys. Rev. **48**, 84 (1935).
[20] K. I. Okazaki, Y. Nakato, and K. Murakoshi, Phys. Rev. B **68**, 035434 (2003).
[21] N. M. Hugenholtz and L. Van Hove, Physica **24**, 363 (1958).
[22] K. Morawetz, N. H. March, and R. H. Squire, Phys. Lett. A **372**, 1707 (2008).
[23] M. Brack, Helv. Phys. Acta **58**, 715 (1985).
[24] M. S. Ferreira, T. G. Dargam, R. B. Muniz, and A. Latge, Phys. Rev. B **63**, 245111 (2001).
[25] M. I. Katsnelson, Mater. Today **10**, 20 (2007).
[26] R. J. Furnstahl, J. Phys. G **31**, S1357 (2005).
[27] S. Suzuki, Y. Watanabe, and S. Heuen, Current Opinion in Solid State and Materials Science 10, 53 (2006).